Technical and Economic Potentialities of the Development of Electric Wind Pumping Systems in the North Region of Cameroon

Dieudonné Kidmo Kaoga, Bachirou Bogno, Michel Aillerie, Kodji Deli

Technical and Economic Potentialities of the Development of Electric Wind Pumping Systems in the North Region of Cameroon

Dieudonné Kaoga Kidmo[1,*], Bachirou Bogno[1,2,3], Michel Aillerie[2,3,*], Kodji Deli[1]
1- University of Maroua, P.O.Box 46 Maroua, Cameroon
2- Université de Lorraine, LMOPS-EA 4423, 570770, Metz, France
3- CentraleSupelec, LMOPS LMOPS-EA 4423, 570770, Metz, France
*Corresponding author: kidmokaoga@gmail.com, aillerie@metz.supelec.fr

---

ABSTRACT

In the present work, the potential of wind electric pumping systems (WEPS) utilization has been investigated for eight localities of the North Region of Cameroon, using long-term satellite-derived data and measured data at 10 m height above ground level (agl). Statistical indexes of accuracy performed the comparison between measured and satellite-derived data. The results suggested that satellite-derived data can accurately represent measured data. Furthermore, satellite-derived data can be suitable to assess the wind resource when measured ground level data are missing. The two-parameter Weibull Probability distribution function (PDF) and parabolic law were utilized, respectively to model wind speeds characteristics and wind turbines power curve. Four wind turbines (WT), represented by WT_1, WT_2, WT_3 and WT_4, with a rated capacity of 20 kW and a 30 m tower, were considered to simulate the power output and energy produced. The results showed that annual power densities at 10 m agl, for Bashéo, Beka, Figuil, Garoua, Pitoa, Poli, Rey-Bouba and Touboro were, respectively, 29.74, 17.45, 33.64, 17.94, 22.28, 11.99, 16.46 and 15.98 W/m^2, while corresponding energy densities were 0.71, 0.42, 0.81, 0.43, 0.53, 0.29, 0.40 and 0.38 kWh/m^2/day, in that order. Annual average frequencies for wind speeds greater or equal to WT's cut-in wind speeds for each of the eight sites were determined. The greatest probability of observing higher wind speeds is for the site of Figuil, .This site showed the best combination of capacity factors (CF), costs of energy (COE), costs of water (COW) and flow rate capacity, At the opposite, the greatest probability of observing lower speeds is for the site of Poli that displayed the worst values of CF, COE, COW and flow rate capacity independently of the WT used. As a result, choosing WT for low wind speeds sites, would require to combine location wind resource and WT characteristics such as cut-in and rated wind speeds in order to take full advantage of costs of energy and water produced.

1- INTRODUCTION

Energy is one of the indispensable inputs for economic development and social prosperity of humankind. With current consumption patterns on a global scale, fossil fuels supply shortages are highly expected to occur in the near future if present trends continue. These consumption patterns connote the importance of shifting focus towards renewable energy for a sustainable development. Renewables consumption in Cameroon as well as in the vast majority of sub-Saharan Africans countries, are insignificant, despite the huge potential, essentially untapped [1].

Wind power generation has achieved a double-digit growth figure for the past 20 years, with an average growth rate of 22%. Nowadays, wind power is a mature and cost-competitive technology for electricity production that can be considered a reliable means to supply energy to populations, mainly in remote locations[2]. Wind power systems require to accurately characterize the wind resource over the country in addition to its geographic distribution[3].

Satellite-based wind resource are valuable datasets in Cameroon as well as in many other sub-Saharan Africans countries, where very few meteorological stations located at main airports are available, and where studies on wind power remain very limited. Several studies have been published in scientific literature related to the use of long-term satellite-derived data and their accuracy in comparison with in situ measurements [4–7]. The objective of this work is to acknowledge the use of satellite-based wind resource as appropriate to provide a reasonable assessment, before higher-accuracy on location measurements are accessible.

The present paper explores wind energy generation using electric systems for water pumping in the North region of Cameroon. Ground measurements at 10 m height above ground level (agl), in hourly time-series format, from January 2007 to January 2012 were collected through a cup-generator anemometer for the site of Garoua. Satellite-derived data for the sites of Bashéo, Beka, Figuil, Pitoa, Poli, Rey-Bouba and Touboro, where measured ground level data remained non-existent, were obtained from the NASA Langley Research Center (LaRC) POWER Project funded through the NASA Earth Science/Applied Science Program[8]. The accuracy of satellite-derived data for Garoua (the only site with ground measurements) were assessed using statistical indexes of accuracy, namely mean bias error (MBE), root mean square error (RMSE), relative root mean square error (RRMSE), coefficient of determination (R^2) and index of agreement (IOA). The two-parameter Weibull probability distribution function and parabolic law were utilized, respectively to model wind speeds characteristics and WT power curve. Four WT were considered to simulate the power output and energy produced. Furthermore, the cost of energy generated (XAF/kWh) and water produced (XAF/m^3) were estimated using the Present Value Cost (PVC) method of energy produced per year, considering the frequency at which WT produce power. The novelty, with respect to the use of long-term satellite-derived wind speed data as well as statistical indexes of accuracy for comparison with available ground measurements, consists in exploring wind resource and characteristics of pitch-regulated WT to take full advantage of costs of energy and water produced.

2- METHODOLOGY

Description of the North Region of Cameroon

The North Region as shown in Fig. 1, is one of the ten regions of Cameroon. Located between 7.30N - 10N latitude and 12.30 - 15.0E longitude, It covers an area of 66,090 km² and is bordered by two regions of the country, the Far North Region to the north and the Adamawa Region to the south, Chad to the east, Central African Republic to the southeast and Nigeria to the west. The North region accounts for one of the driest regions of Cameroon under the influence of the harmattan winds in the dry season which lasts four months, temperatures rise at their highest (40 – 45°C) and there is no rainfall. During the rainy season which lasts four months, average rainfall is between 900–1500 mm and torrential rains are observed as well as lower temperatures compared to dry season. The Benoue depression constitutes the primary land feature of the North region, with an elevation in the range of zero to 200 meters. Land elevations are in the range of 200–500 and 500–1000 meters, respectively in the north and south of the region [9]. The selected sites, namely, Bashéo, Beka, Figuil, Garoua, Pitoa, Poli, Rey-Bouba and Touboro have been chosen based on relevant landscape information they provide in order to fully to assess the potential of wind energy in the north Region of Cameroon.

Wind Data Description and Source

Two sources of data have been utilized in this work, measurements from a ground station for the site of Garoua and long-term satellite-derived data for the seven other sites. Wind speed measurements for the locality of Garoua, at 10 m height above ground level (agl), in hourly time-series format, from January 2007 to January 2012 have been collected through a cup-generator anemometer at the Garoua, main meteorological station[10]. For the seven other selected sites of the north region, measured ground level data are non-existent. Therefore, long-term daily satellite-derived data, from January 2005 to January 2020, obtained through the POWER, have been utilized. These data were obtained from the NASA Langley Research Center (LaRC) POWER Project funded through the NASA Earth Science/Applied Science Program[8]. Table 1 provides geographical coordinates of the eight sites, as well as mean ambient temperature and measurement period.

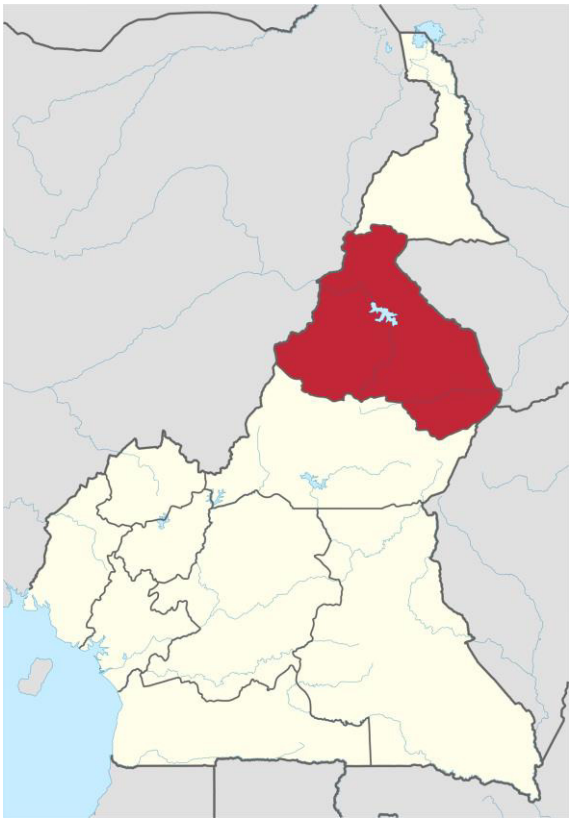

FIGURE 1. Map showing the North region of Cameroon[9].

TABLE 1. Geographical data for eight selected sites of the North Region.

Location	**Latitude (°)**	**Longitude (°)**	**Elevation (m)**	**Ambient temperature (°C)**	**Measurement period**
Bashéo	9.6721	13.3711	403.8	27.47	Jan 2005 - Jan 2020
Beka	9.0437	12.8982	296.16	27.90	Jan 2005 - Jan 2020
Figuil	9.7524	13.976	407.05	27.67	Jan 2005 - Jan 2020
Garoua Ier	9.2955	13.3998	291.79	28.19	Jan 2005 - Jan 2020
Lagdo	9.2862	13.3766	291.79	28.19	Jan 2005 - Jan 2020
Poli	8.4785	13.2595	512.62	26.67	Jan 2005 - Jan 2020
Rey-Bouba	8.6633	14.1595	344.08	28.17	Jan 2005 - Jan 2020
Touboro	7.7739	15.3489	651.63	25.96	Jan 2005 - Jan 2020

Mean Wind Speed and Standard Deviation

Monthly mean wind speed v_m and standard deviation σ of wind speed data are calculated as Eqs. 1 & 2:

$$v_m = \frac{1}{N}\left(\sum_{i=1}^{N} v_i\right) \quad \textbf{(1)}$$

$$\sigma = \left[\frac{1}{N-1}\sum_{i=1}^{n}(v_i - v_m)^2\right]^{1/2} \quad \textbf{(2)}$$

Where:

v_m = mean wind speed $[m/s]$
σ = standard deviation of the mean wind speed $[m/s]$
v_i= wind speed $[m/s]$
N = number of wind speed data.

After the statistical analysis of wind data, monthly mean wind speeds and standard deviations for Garoua using measured and satellite-derived data, are summarized in Table 2, while Fig.2 shows the corresponding values using only satellite-derived data, for the eight selected sites. The magnitude of the monthly mean measured wind speeds and standard deviations for Garoua at 10 m height above agl, lay respectively within the range of 1.237 to 2.711 m/s and 0.733 to 1.385 m/s, while corresponding values using satellite-derived data range from 1.67 to 3.38 m/s and from 0.47 to 1.00 m/s, in that order

TABLE 2. Monthly mean wind speeds and standard deviations for Garoua using measured and satellite-derived data.

PERIOD	Measured		Satellite-derived	
	v_{mG}	σ_G	v_{mS}	σ_S
JAN	1.585	0.920	3.21	0.84
FEB	1.588	0.930	3.38	0.95
MAR	2.093	1.057	3.35	1.00
APR	2.711	1.385	3.09	0.92
MAY	2.511	1.256	2.54	0.69
JUN	2.492	1.296	2.31	0.74
JUL	2.333	1.287	2.22	0.66
AUG	1.840	1.017	2.04	0.63
SEP	1.603	0.884	1.67	0.47
OCT	1.583	0.949	1.70	0.49
NOV	1.395	0.870	2.21	0.64
DEC	1.237	0.733	2.88	0.70
WHOLE YEAR	1.915	1.168	2.55	0.68

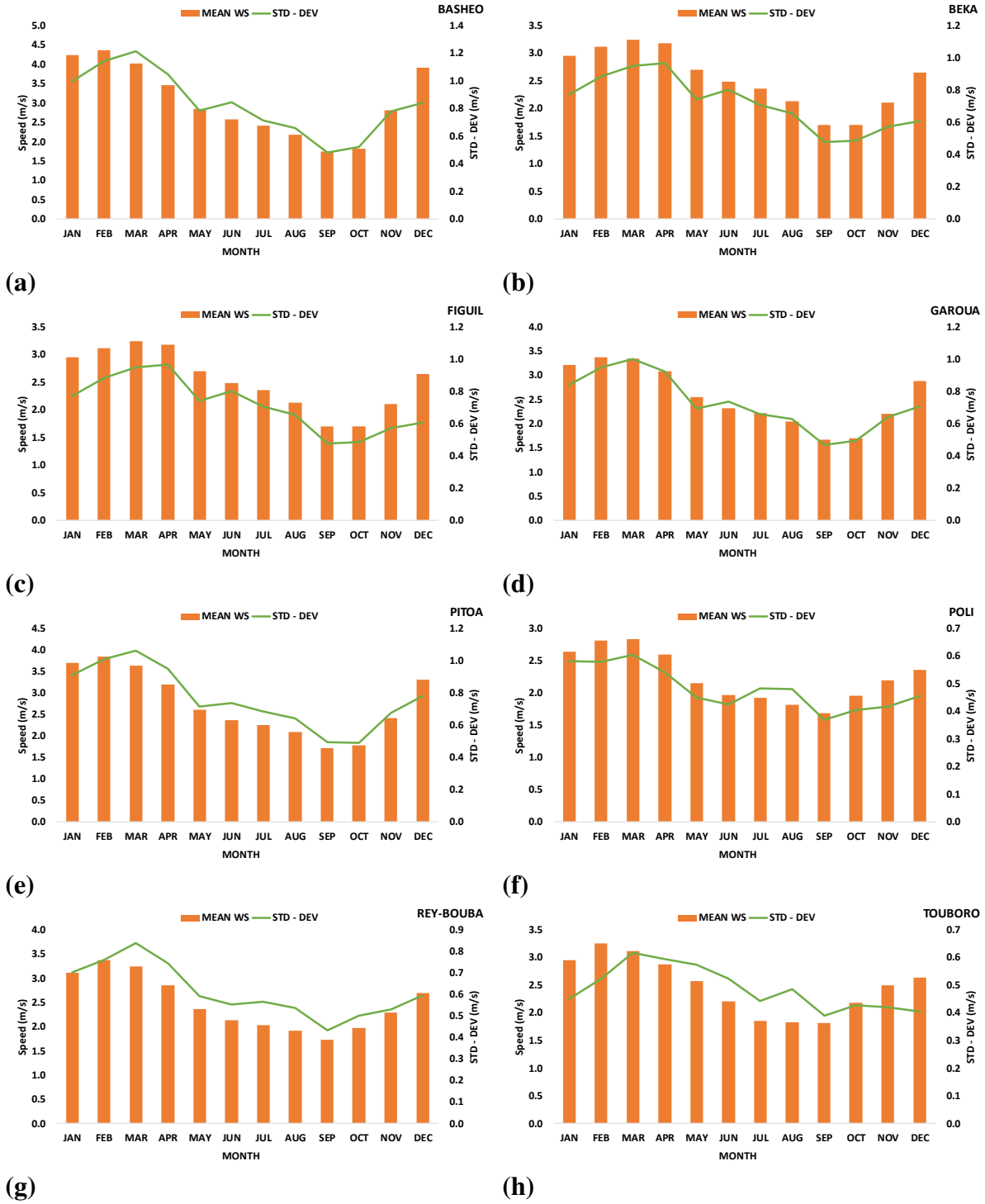

FIGURE 2. Monthly mean wind speeds and standard deviations using ground and satellite-derived data for (a) Bashéo, (b) Beka, (c) Figuil, (d) Garoua, (e) Pitoa, (f) Poli, (g) Rey-Bouba and (h) Touboro.

Weibull Probability Density Function

The Weibull probability density function (PDF), which is a special case of a generalized two-parameter Gamma distribution, has been extensively utilized in scientific literature for wind speed forecasting and wind energy potential assessment[11–13]. Weibull PDF can be

characterized by its PDF $f(V)$ using Eq. 3 and cumulative distribution function (CDF), $F(V)$ using Eq. 4 [14]:

$$f(v) = \left(\frac{k}{C}\right).\left(\frac{v}{C}\right)^{k-1}.\exp\left[-\left(\frac{v}{C}\right)^{k}\right] \quad \textbf{(3)}$$

$$F(v) = 1 - \exp\left[-\left(\frac{v}{C}\right)^{k}\right] \quad \textbf{(4)}$$

Where: $f(v)$ *= probability of observing wind speed* v *;* v *= wind speed* $[m/s]$*;* C *= Weibull scale parameter* $[m/s]$*;* k *= Weibull shape parameter.*

Weibull parameters k and C are typically obtained using well-established estimation methods[10]. In this paper, Weibull parameters are computed using the energy pattern factor method (E_{pf} method) with E_{pf} is defined first as Eq. 5 [15–17] :

$$E_{pf} = \frac{(v^3)_m}{(v_m)^3} = \frac{\left(\frac{1}{n}\sum_{i=1}^{n} {v_i}^3\right)}{\left(\frac{1}{n}\sum_{i=1}^{n} v_i\right)^3} \quad \textbf{(5)}$$

Once the E_{pf} is computed, the shape parameter is estimated using Eq. 6:

$$k = 1 + \frac{3.69}{(E_{pf})^2} \quad \textbf{(6)}$$

The scale parameter is obtained using Eq. 7:

$$C = \frac{v_m}{\Gamma\left(1+\frac{1}{k}\right)} \quad \textbf{(7)}$$

Statistical indexes of accuracy

In order to evaluate the accuracy of satellite-derived data for the site of Garoua, the following statistical indexes of accuracy are utilized:

1. Mean Bias Error of satellite-derived values using Eq. 8 [18,19] :

$$MBE = \left[\frac{1}{N}\sum_{i=1}^{N}(Sat_i - Gr_i)^2\right]^{1/2} \quad \textbf{(8)}$$

where Gr_i denotes cumulative frequency distribution (CFD) of measured values at wind speed v_i, in time step i, Sat_i the respective satellite-derived value, and N the number of non-zero wind speed data points. MBE provides basically the difference between CFD of average satellite-derived and average measured values. Satellite-derived values are overestimated if $MBE > 0$, while they are underestimated if $MBE < 0$.

2. Root mean square error (RMSE) using Eq. 9 [20,21]:

$$RMSE = \left[\frac{1}{N}\sum_{i=1}^{N}(Sat_i - Gr_i)^2\right]^{1/2} \quad \textbf{(9)}$$

RMSE provides the deviation between satellite-derived and measured values. Successful forecasts correspond to low values of RMSE, while higher indicate deviations[19]. RMSE should be as close to zero as possible.

3. Relative root mean square error (RRMSE) using Eq. 10 [11,22] :

$$RRMSE = \frac{\left[\frac{1}{N}\sum_{i=1}^{N}(Sat_i - Gr_i)^2\right]^{1/2}}{\frac{1}{N}\sum_{i=1}^{N} Gr_i} \times 100 \quad \textbf{(10)}$$

RRMSE is calculated by dividing RMSE to the average of CFD of measured values. Ratings of satellite-derived values' accuracy can be defined as[23] :

Excellent : RRMSE < 10%;
Good : 10% < RRMSE < 20%;
Fair : 20% < RRMSE < 30%;
Poor : RRMSE > 30%.

4. Coefficient of determination (R^2) using Eq. 11 [11,24]:

$$R^2 = 1 - \frac{\sum_{i=1}^{N}(Gr_i - Sat_i)^2}{\sum_{i=1}^{N}(Gr_i - \overline{Sat_i})^2} \quad \textbf{(11)}$$

R^2 determines the linear relationship between CFD of average satellite-derived and average measured values. A higher R^2 represents a better fit using satellite-derived data and the highest value it can get is 1.

Where: Gr_i is the i^{th} CFD of ground (measured) wind speeds, Sat_i is the i^{th} CFD of satellite-derived wind speeds, $\overline{Sat_i}$ is the mean value of Sat_i, N the number of non-zero wind speed data points.

5. Index of Agreement (IOA) using Eq. 12 [11,25]:

$$IOA = 1 - \frac{\overline{Sat_i} - \overline{Gr_i}}{\sum_{i=1}^{N}(|Sat_i - \overline{Gr_i}| + |Gr_i - \overline{Gr_i}|)^2} \quad \textbf{(12)}$$

Where: $\overline{Gr_i}$ denotes the average of Gr_i, $\overline{Sat_i}$ is the mean value of Sat_i, N the number of non-zero wind speed data points. IOA estimates the accuracy of satellite-derived wind speeds in predicting ground (measured) wind speeds. IOA values range from zero to one. IOA values above 0.5 imply efficiency in using satellite-derived data[19]

Extrapolation of Wind Speeds at Different Hub Heights

In this study, four WT, using a 30m hub height have been considered. Wind speeds data obtained at 10 m height agl, are therefore adjusted to the relevant WT hub height. The vertical extrapolation of scale and shape parameters at an elevation more than 10 m, is defined by the relationships in Eqs. 13 & 14 [26,27]:

$$C_z = C_{10} * \left(\frac{z}{z_{10}}\right)^n \quad \textbf{(13)}$$

$$k_z = \frac{k_{10}}{1 - 0.00881\, ln(z/10)} \quad \textbf{(14)}$$

Where z and z_{10} are in meters and the power law exponent n is given by Eq. 15:

$$n = [0.37 - 0.088\, ln(C_{10})] \quad \textbf{(15)}$$

Where, the scale C_{10} and shape k_{10} parameters are determined at 10 m height agl.

Power Curve Model and Capacity Factor

The power curve model of a WT can be modelled by four parameters: the cut-in wind speed (v_c), the rated wind speed (v_R), the cut-off wind speed (v_F) and the rated electrical power (P_{eR}).

In this study, the power output curve model of a WT can be approximated with the parabolic law, using the combination of Eq. 16 [28]:

$$P_e = \begin{cases} 0 & (v < v_c) \\ P_{eR}\frac{v^k - {v_c}^k}{{v_R}^k - {v_c}^k} & v_c \le v \le v_R \\ P_{eR} & v_R \le v \le v_F \\ 0 & (v_F < v) \end{cases} \quad \textbf{(16)}$$

The average power output ($P_{e,ave}$) from the turbine, which is related to the total energy production can be determined from Weibull distribution as Eq. 17:

$$P_{e,ave} = P_{eR}\left\{\frac{e^{-\left(\frac{v_c}{C}\right)^k} - e^{-\left(\frac{v_R}{C}\right)^k}}{\left(\frac{v_R}{C}\right)^k - \left(\frac{v_c}{C}\right)^k} - e^{-\left(\frac{v_F}{C}\right)^k}\right\} \quad \textbf{(17)}$$

The capacity factor CF is defined as the ratio of the average power output ($P_{e,ave}$) to the rated electrical power (P_{eR}) of the WT. The capacity factor CF can thus be computed as Eq. 18 [29]:

$$CF = \left\{\frac{e^{-\left(\frac{v_c}{C}\right)^k} - e^{-\left(\frac{v_R}{C}\right)^k}}{\left(\frac{v_R}{C}\right)^k - \left(\frac{v_c}{C}\right)^k} - e^{-\left(\frac{v_F}{C}\right)^k}\right\} \quad \textbf{(18)}$$

Water Pumping Capacity

The net hydraulic power output (P_{out}) required to deliver a volume of water $V_w(m^3)$ can be expressed using Eq. 19 [30]:

$$P_{out} = \frac{\rho_w \cdot g \cdot V_w \cdot H}{\eta T} = \frac{\rho_w \cdot g \cdot Q_w \cdot H}{\eta} \quad \textbf{(19)}$$

Where: $Q_w = volumetric\ flow\ rate\ [m^3/day]$;
ρ_w = *water density* $[kg/m^3]$;
g = *acceleration due to gravity* $[m/s^2]$;
H = *pump head* $[m]$; η = *system efficiency.*

The volumetric flow rate of water is therefore evaluated using Eq. 20:

$$Q_w = \frac{\eta \cdot P_{out}}{\rho_w \cdot g \cdot H} \quad \textbf{20)}$$

When taking into account the efficiency of the pump ($\eta_{PUMP} = 62\%$ for the submersible electric pump model) the water pumping capacity rate (F_w) can be expressed as Eq. 21 :

$$F_w = 367 \times \eta_{PUMP} \cdot P_{out} \quad \textbf{(21)}$$

Costs Analysis

In this work, the adopted method to evaluate the costs of energy (COE) and costs of water (COW) produced is the present value of costs (PVC) of energy produced per year using Eq. 22 [31] **:**

$$PVC = I + C_{om}\left(\frac{1+i}{r-i}\right) * \left(1 - \left(\frac{1+i}{1+r}\right)^n\right) - S\left(\frac{1+i}{1+r}\right)^n \quad \textbf{(22)}$$

Where the following assumptions are made to estimate the cost of energy produced by the considered WT:

- ***I*** is the investment cost, which includes the WT price in addition to 20% for civil works and other connections;

- Average specific WT cost per kW is USD 1175, for WT rated power between 20 and 200 kW[32]
- $\boldsymbol{n}$ is the useful lifetime of WT in years (20 years); $\boldsymbol{i_o}$ is the nominal interest rate (16%);
- $\boldsymbol{S}$ is the scrap value (10% of the WT price); $\boldsymbol{i}$ is the inflation rate (3.6%);
- $\boldsymbol{C_{om}}$ is the operation and maintenance costs (7.5% of the investment cost).

The discount rate ($\boldsymbol{r}$) is determined using Eq. 23 [33] :

$$\boldsymbol{r = \frac{i_0 - i}{1 + i}} \quad \textbf{(23)}$$

The Wind availability (A) is determined using Weibull CDF of wind speeds at which WT produce energy. The total energy output (E_{WT}) over the WT lifetime (in kilowatt-hour) is computed as Eq. 24:

$$E_W = 8760 * A * n * P_R * C_f \quad \textbf{(24)}$$

The cost of energy (COE) per unit kWh using the PVC method can be estimated using Eq. 25:

$$COE = \frac{PVC}{E_W} \quad \textbf{(25)}$$

The annual volume of water V_w (m^3/year) produced by the WT is determined from Eq. 26:

$$V_w = \frac{\eta \cdot E_w}{n \cdot \rho_w \cdot g \cdot H} \quad \textbf{(26)}$$

The cost of water (COW) per unit m^3 using the PVC method can be estimated using Eq. 27:

$$COW = \frac{PVC}{n \cdot V_w} \quad \textbf{(27)}$$

3- RESULTS AND DISCUSSION

Weibull PDF and CDF 10 m Height agl (Measured Vs Satellite Data)for Garoua

Figure 3 show the Weibull PDF plots for the monthly average at 10 m height agl, using respectively, measured and satellite-derived data, while Fig. 4 presents the corresponding values for the Weibull CDF plots. Average monthly Weibull CDF values helped to perform the statistical comparison between measured and satellite-derived data. Table 3 shows statistical indicators for the accuracy of satellite-derived wind speed for the site of Garoua, which is the only site with measured ground level data. With the exception of May, June and July, satellite-derived values are slightly overestimated ($MBE > 0$) for the rest of the year as the yearly average MBE value of 0.021 indicates a slight overestimation of satellite-derived data for the concerned months. Nevertheless, MBE values can be considered in all cases close to zero, which demonstrate a good match between locally measured and long-term satellite-derived data. Considering the RMSE values, they range between 0.142 in February and 0.002 in May and thus, being close to zero, pointing out successful forecasts. RRMSE values, from April to November, are less than 10%, denoting an excellent accuracy of satellite-derived data. RRMSE values for January, February, March and December are good, with values ranging from 11.4% to 15.5%. Overall, the accuracy of satellite-derived data for yearly average is excellent, with a RRMSE value of 6.1%. R^2 values vary from 0.847 in May to 0.696 in December. R^2 value of the yearly average is 0.809. R^2 values are generally higher and

represents a better fit using satellite-derived data. IOA values range between 0.993 and 1.000 and this implies efficiency in using satellite-derived data. Therefore, satellite-derived data can accurately represent measured data and when measured ground level data are missing, satellite-derived data can be suitable to assess the potential of wind energy. Similar studies on the use of satellite-derived data are found in the literature. Schmidt et al [7] performed a comparison between in situ measurements of wind speed from Wave Glider (WG) and satellite/reanalysis products, including the wind speed error per wind speed category, RMSE, bias, and correlation coefficients. Accuracy values are within the same ranges as the present work. Barthelmie and Pryor [5] worked on satellite sampling of offshore wind speeds to represent wind speed distributions. Their study have stressed the difficulties to obtain through in situ methods wind speeds over the oceans. Remmers T et al [6] observed a very strong positive linear relationship between satellite-derived wind speed data and the in situ measurements. Ayompe LM, Duffy A.[34] assessed the energy generation potential of photovoltaic systems in Cameroon using satellite-derived solar radiation datasets due to the lack of a reliable network of surface observation stations for collecting weather data in the country. These studies concluded that the accuracy of satellite-derived data varies according to empirical model functions utilized. Besides, the accuracy of satellite-based wind resource is sufficient to provide a reasonable assessment in the initial phase of wind project planning, before higher-accuracy in situ measurements are available.

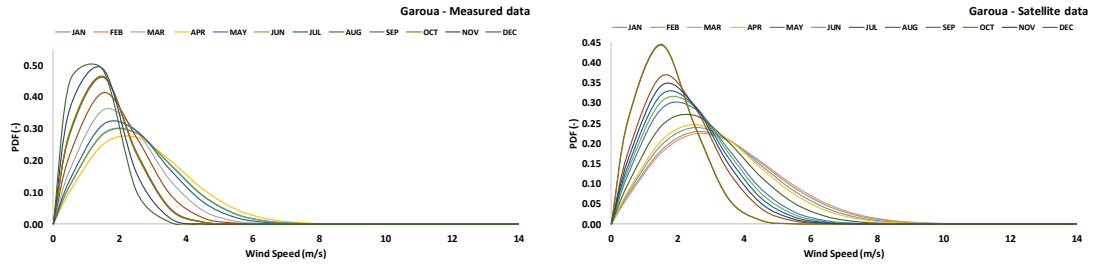

FIGURE 3. Monthly average PDF at 10 m height agl for Garoua using (a) measured data and (b) satellite-derived data.

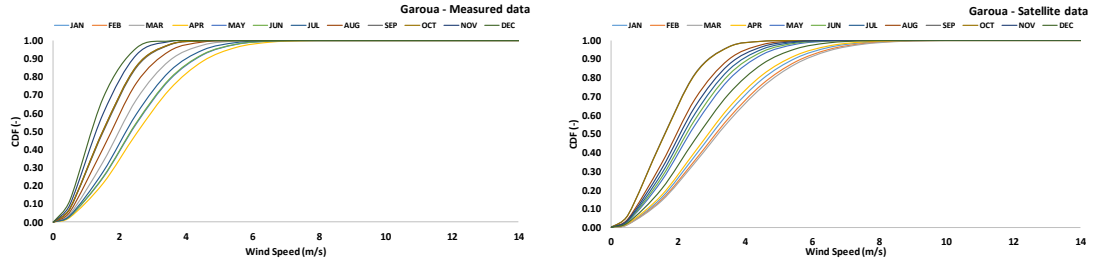

FIGURE 4. Monthly average CDF at 10 m height agl for Garoua using (a) measured data and (b) satellite-derived data.

TABLE 3. Statistical indicators for the accuracy of satellite-derived wind speed for Garoua.

PERIOD	MBE	RMSE	RRMSE	R^2	IOA
JAN	0.053	0.133	14.6%	0.759	0.993

FEB	0.058	0.142	15.5%	0.757	0.993
MAR	0.043	0.103	11.4%	0.805	0.995
APR	0.012	0.029	3.2%	0.841	0.999
MAY	- 0.001	0.002	0.2%	0.847	1.000
JUN	- 0.003	0.009	1.0%	0.848	1.000
JUL	- 0.001	0.004	0.4%	0.843	1.000
AUG	0.007	0.021	2.3%	0.813	0.999
SEP	0.003	0.008	0.9%	0.792	1.000
OCT	0.004	0.011	1.2%	0.789	1.000
NOV	0.026	0.077	8.3%	0.745	0.996
DEC	0.051	0.139	15.0%	0.696	0.993
YEARLY	0.021	0.056	6.1%	0.809	0.998

Wind Characteristics

Wind Characteristics at 10 m Height agl

Figure 5 presents yearly average PDF and CDF at 10 m height agl for the eight sites using long-term satellite-derived data. From the PDF figure, it can be seen that the probability of observing higher wind speeds is highest for the sites of Figuil and Pitoa. In addition, the probability of observing lower wind speeds is highest for the site of Poli.

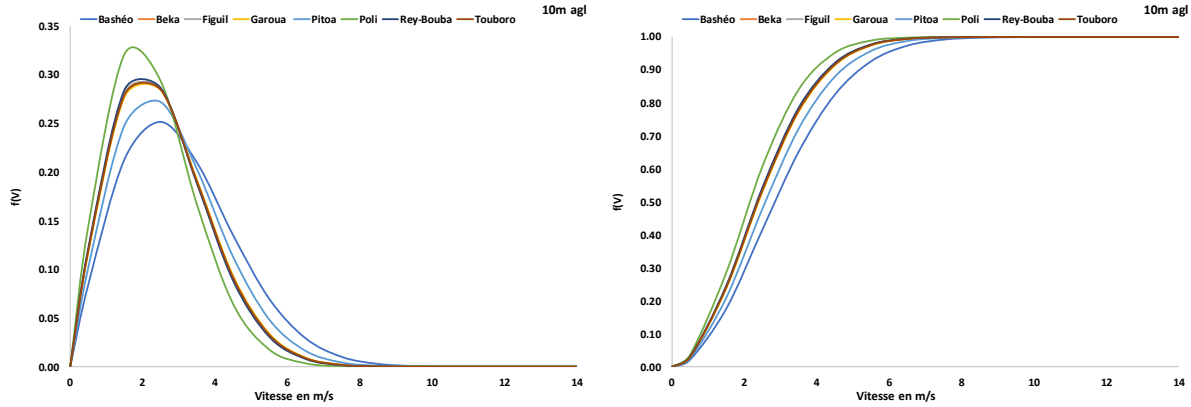

FIGURE 5. Yearly average PDF (a) and CDF (b) at 10 m height agl for the eight sites of the North Region

Statistical Weibull analysis of the eight sites' wind speed data at 10 m height agl, gave the results of Table 4. For each site, the average air density is based on daily average temperature and location values of elevation. Air density values in the North Region vary between 1.10 and 1.13 kg/m^3, while the corresponding elevations are in the range of 291.79 - 651.63 m. Annual average wind speeds range from 2.24 m/s for Poli to 3.16 m/s for Figuil, corresponding wind power densities vary from 8.43 W/m² for Poli to 28.89 W/m² for Figuil. With annual average wind power densities less than 100 W/m², the wind resource in the North Region can be ranked as wind power class 1, based on the scheme proposed by Battelle—Pacific Northwest

Laboratory (PNL)[35]. Class 1 areas are considered are unsuitable for large scale wind power development.

TABLE 4. Annual wind characteristics at 10 m agl for the eight sites.

Location	$\boldsymbol{\sigma}$ $(\boldsymbol{m/s})$	**k (-)**	$\boldsymbol{C(m/s)}$	$\boldsymbol{V_m}$ $(\boldsymbol{m/s})$	$\boldsymbol{\rho}$ $(\boldsymbol{kg/m^3})$	$\boldsymbol{W_{PD}(W/m^2)}$	$\boldsymbol{E_{PD}}$ $\boldsymbol{(kWh/m^2/day)}$
Bashéo	1.00	2.43	3.42	3.03	1.12	25.09	0.60
Beka	0.60	2.76	2.84	2.53	1.13	13.48	0.32
Figuil	1.12	2.37	3.56	3.16	1.12	28.89	0.69
Garoua	0.68	2.63	2.87	2.55	1.13	14.29	0.34
Pitoa	0.82	2.54	3.09	2.74	1.13	18.19	0.44
Poli	0.43	3.27	2.50	2.24	1.11	8.43	0.20
Rey-Bouba	0.61	2.89	2.78	2.48	1.13	12.30	0.30
Touboro	0.54	3.32	2.77	2.48	1.10	11.15	0.27

wind characterisitic on the 8 sites

Figure 6 illustrates annual average PDF and CDF plots for 30 m elevation for the eight sites. It can be observed from Fig. 6 that, for each of the eight sites, the peak of the PDFs, which indicates the most frequent wind speed, skews towards the higher values of wind speed. It can further be observed that

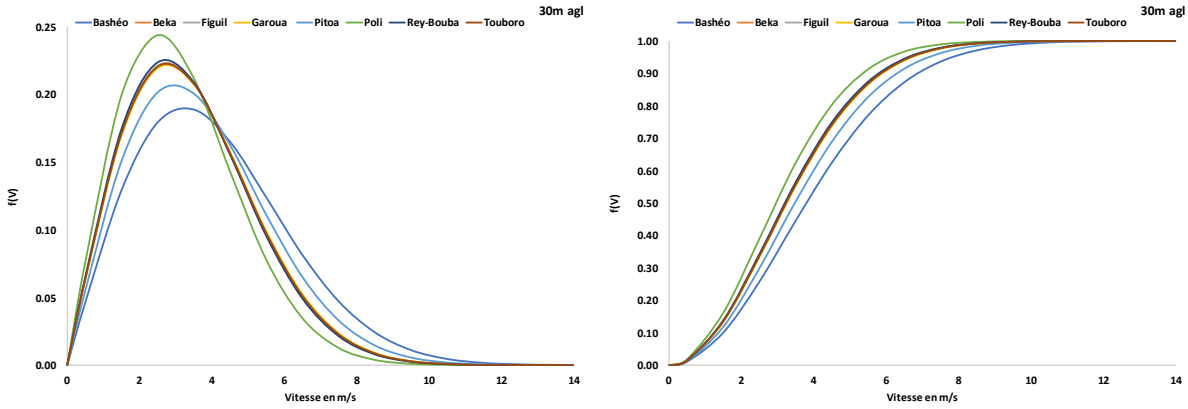

(a) **(b)**

FIGURE 6. Annual average PDF (a) and CDF (b) at 30 m height agl (30m_hub height) for the eight sites.

Table 5 proposes statistical Weibull analysis of wind speed data for 30 m elevation (tower of WT) for the eight sites. For each site, the average air density was adjusted to reflect the 30m-

hub height tower. Annual average Weibull parameters were extrapolated to the 30 m height agl, as well as average wind speeds, power densities and energy densities.

TABLE 5. Annual wind characteristics at WT's hub height for the eight sites.

Location	k (-)	$C(m/s)$	V_m (m/s)	ρ (kg/m^3)	$W_{PD}(W/m^2)$	E_{PD} $(kWh/m^2/day)$
Bashéo	2.43	4.55	4.04	1.12	59.35	1.42
Beka	2.76	3.85	3.43	1.13	33.65	0.81
Figuil	2.37	4.73	4.19	1.12	67.52	1.62
Garoua	2.63	3.89	3.46	1.13	35.55	0.85
Pitoa	2.54	4.16	3.69	1.13	44.30	1.06
Poli	3.27	3.44	3.08	1.11	21.83	0.52
Rey-Bouba	2.89	3.78	3.37	1.12	30.88	0.74
Touboro	3.32	3.76	3.38	1.09	28.04	0.67

Table 6 presents for WT_1, WT_2, WT_3 and WT_4 , the annual average frequency for wind speeds greater or equal to WT's cut-in wind speed for each of the eight sites of North Region. From the PDF figure, it can be seen that the probability of WT to produce power is the highest using WT1, while this availability is the lowest using WT_4.

TABLE 6. Annual average frequency for wind speeds greater or equal to WT cut-in wind speed for different sites.

Location	WT1	WT2	WT3	WT4
Bashéo	87.34%	79.23%	69.58%	69.58%
Beka	84.90%	73.86%	60.59%	60.59%
Figuil	87.84%	80.24%	71.23%	71.23%
Garoua	84.10%	73.22%	60.42%	60.42%
Pitoa	85.59%	76.01%	64.66%	64.66%
Poli	84.37%	70.31%	52.77%	52.77%
Rey-Bouba	85.29%	73.85%	59.87%	59.87%
Touboro	88.45%	77.31%	62.42%	62.42%

Conclusion partielle

Wind turbine and electric pumping systems (WEPS)

Table 7 provides relevant characteristics of four WT selected for this work. In order to highlight WT characteristics needed for low wind speeds location, the four WT, with a rated capacity of 20 kW and a 30 m tower hub height, were considered for uniformity in the comparison. These WT are represented by WT_1, WT_2, WT_3 and WT_4, to avoid the use of trade names. Cut-in and rated wind speeds are different for each of the four WT. WT_1 has the lowest cut-in and rated wind speeds, while WT_4 has the highest cut-in and rated wind speeds. WT_3 has the same cut-in wind speed as WT_4, but a lower rated wind speed than that of WT_4. WT_2 has higher cut-in and rated wind speed than WT_1, but these values are lower than those of WT_3. Table 5 shows a typical wind electric pumping systems (WEPS). Four 20 kW WT, with characteristics provided in Table 7, with a submersible electric pump model to produce energy from wind and pump water using the produced energy for each of the eight sites of the North Region. For the purpose of this work, a total dynamic head of 25 m was adopted as the average in the North Region. Any other pumping head could be used since the volumetric flow rate of water is inversely proportional to pumping head.

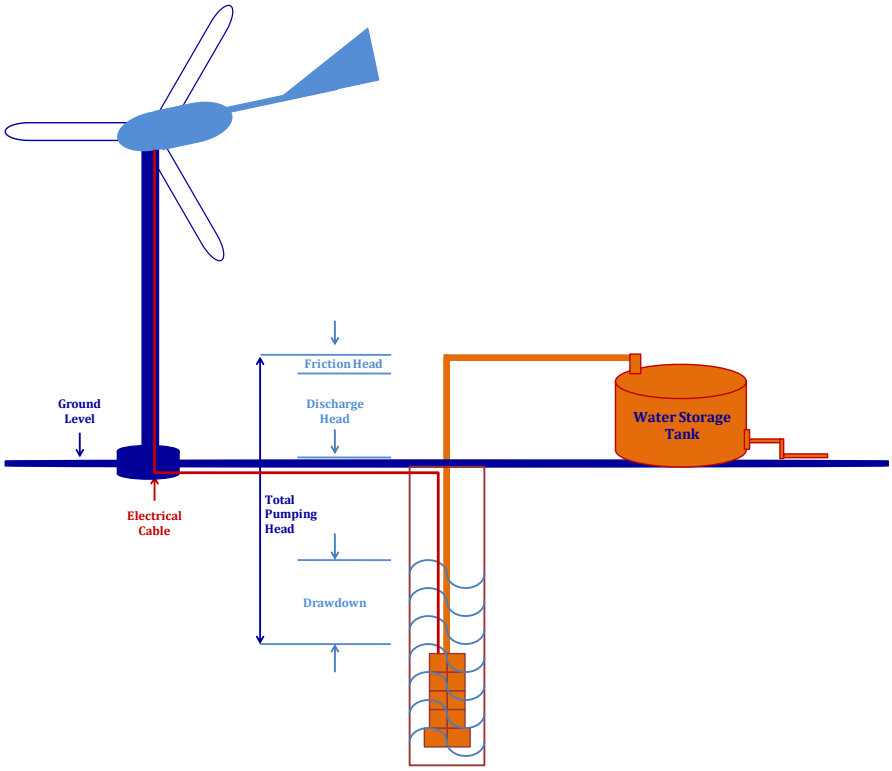

FIGURE 7. Typical wind electric pumping systems (WEPS)

TABLE 7. Characteristics of the selected wind turbines.

Characteristics	**WT_1**	**WT_2**	**WT_3**	**WT_4**
Hub height **(m)**	30	30	30	30
Rated power $\boldsymbol{P_R}$ $\boldsymbol{(kW)}$	20	20	20	20
Rotor diameter **(m)**	10	10	10	10

Cut-in wind speed $\boldsymbol{V_C}$ $(\boldsymbol{m/s})$	2.0	2.5	3.5	3.5
Rated wind speed $\boldsymbol{V_R}$ $(\boldsymbol{m/s})$	10	11	12	13
Cut-off wind speed $\boldsymbol{V_F}$ $(\boldsymbol{m/s})$	25	25	25	25
Price (USD/kW)	1,775	1,775	1,775	1,775
Price (XAF/kW)	1,065,000	1,065,000	1,065,000	1,065,000

Cost of Energy

Figure 8 plots capacity factors (CF) versus costs of energy (COE), using WT_1, WT_2, WT_3 and WT_4, for the eight sites. The site of Figuil shows the best combination of CF and cost of energy, no matter the WT used, followed by the sites of Bashéo and Pitoa. The site of Poli displays the worst CF and COE. For the site of Figuil, the CF is equal to 15.14% and the COE is 93.82 XAF/kWh using the WT_1. For WT_2, CF and COE are, respectively 11.15% and 139,54 XAF/kWh, while for WT_3, the corresponding values are 7.11% and 246.57 XAF/kWh, in that order. WT_4 shows the worst performance, with CF equal to 5.82% and COE equal to 301.05 XAF/kWh

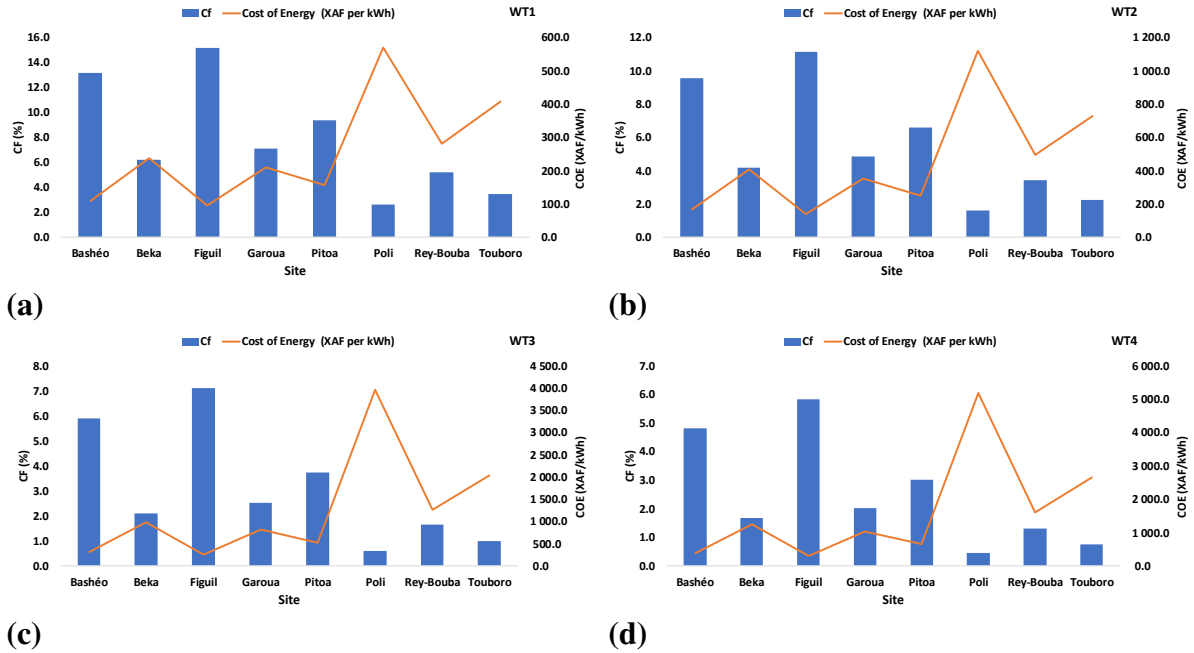

FIGURE 8. CF and COE using WT_1, WT_2, WT_3 and WT_4, for the eight sites

Flow rate capacity

Figure 9 presents annual average flow capacity (m^4/h) for WT_1, WT_2, WT_3 and WT_4 for the eight sites of the North Region. The site of Figuil, based on its higher wind potential, shows the best flow rate capacity and while the site of Poli displays the worst flow rate capacity. For

the site of Figuil, the annual average flow capacity are 613.76, 412.67, 233.55 and 191.28 m^4/h, respectively for for WT_1, WT_2, WT_3 and WT_4.

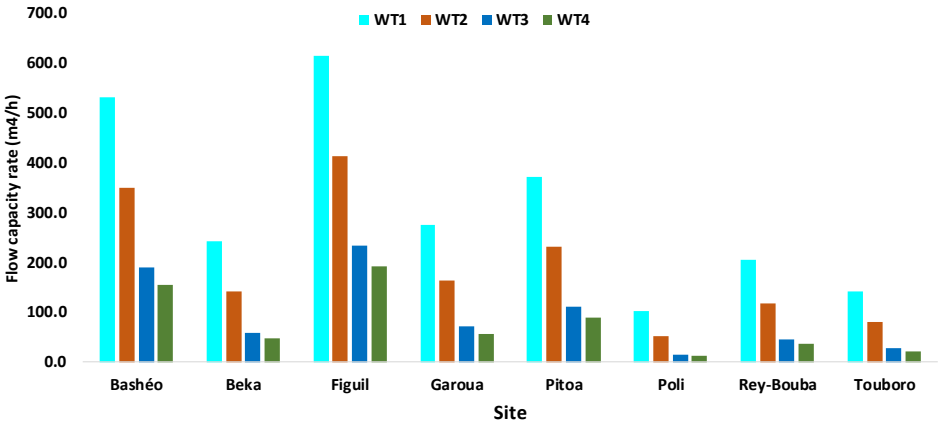

FIGURE 9. Annual average flow capacity (m^4/h) for WT1, WT2, WT3 and WT4 for (a) different sites of the North Region

Cost of Water

Figure 10 illustrates the costs of water (COW) and flow rate (m^3/day), using WT_1, WT_2, WT_3 and WT_4, for the selected sites. Furthermore, the site of Figuil presents the best combination of COW and flow rate energy, while the site of Poli shows the worst values, independently of WT used. For a total dynamic head of 25 m, the COW for site of Figuil are 6.16, 13.64, 42.57 and 63.46 XAF/m^3, respectively using WT_1, WT_2, WT_3 and WT_4, while corresponding values of flow rate energy are 985.38, 445.46, 142.68, 95.71 m^3/day. WT_4, in all cases, shows the poorest performance.

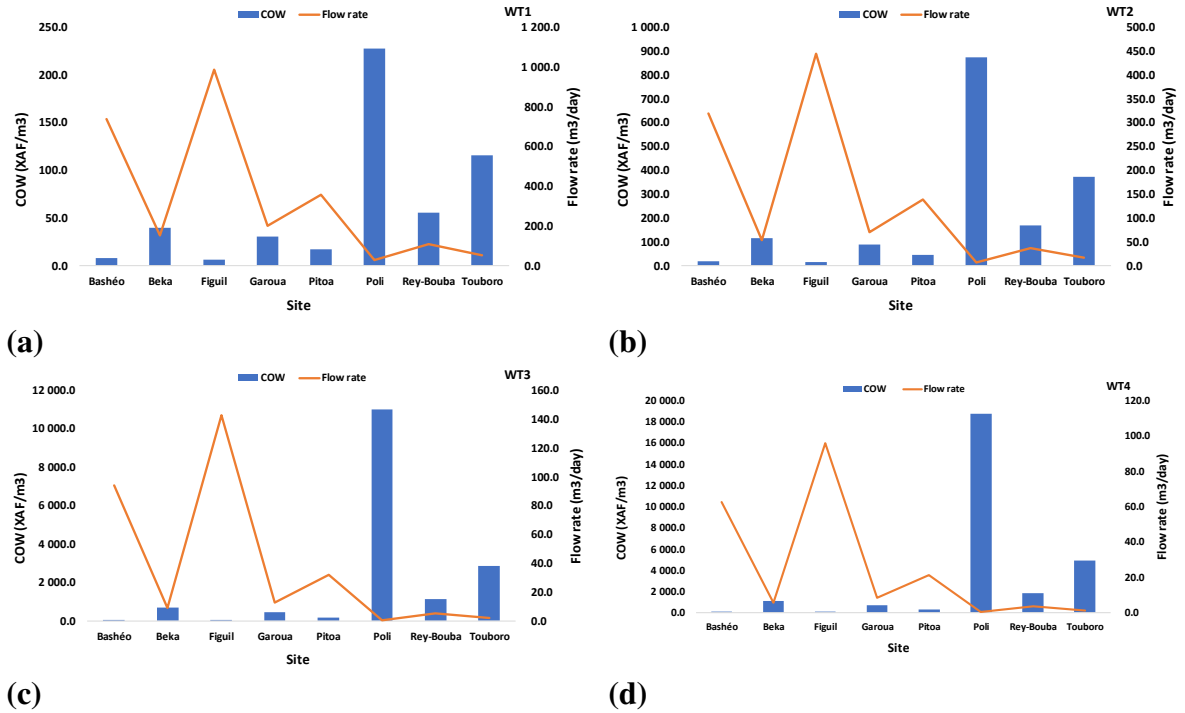

FIGURE 10. COW and volumetric flow rate using WT1, WT2, WT3 and WT4 for eight selected sites

analyse

4- CONCLUSION

The potential of wind energy generation using electric pumping systems in the North region of Cameroon has been explored, using measured wind data and satellite-derived wind data at 10 m height agl. The accuracy of satellite-derived wind speeds data were assessed using MBE, RMSE, RRMSE, R^2 and IOA indicators. The results suggested that the accuracy of satellite-based wind resource is sufficient to provide a reasonable assessment in the initial phase of wind project planning, before higher-accuracy in situ measurements are available. The assessment of the wind resource at 10 m height agl showed average annual power densities in the range of 8.43-28.89 W/m². At 10 m height agl, this wind potential suggests that the North Region falls under class 1 using the scheme proposed by Battelle-Pacific Northwest Laboratory (PNL). Therefore, the wind resource in the North Region is deemed unsuitable for large scale WT applications. Hence, four small scale WT of 20 kW rated power were considered for water pumping applications. Based on its higher performance in comparison to the three other, the WT with the lowest cut-in and rated wind speeds, showed the highest capacity factors, thus the lowest costs of energy and water produced. As a result, cut-in and rated wind speeds have strong impact on the capacity factor, while cut-out wind speed has negligible impact on it. Choosing WT for low wind speeds sites, would require to combine location wind resource and WT characteristics such as cut-in and rated wind speeds in order to take full advantage of costs of energy and water produced.

NOMENCLATURE

$\boldsymbol{v_m}$	Mean wind speed $[m/s]$	$\boldsymbol{v_i}$	Wind speed $[m/s]$
$\boldsymbol{k_{10}}$	Shape parameter at 10 m height agl $[-]$	$\boldsymbol{N}$	Number of wind speed data
$\boldsymbol{k_z}$	Shape parameter at **z** meters height agl $[-]$	$\boldsymbol{v}$	Wind speed [m/s]
$\boldsymbol{\sigma}$	Standard deviation of the mean wind speed $[m/s]$	$\boldsymbol{n}$	Power law exponent $[-]$
$\boldsymbol{n}$	Useful lifetime of WT in years (20 years) $[year]$	$\boldsymbol{v_c}$	Cut-in wind speed $[m/s]$
$\boldsymbol{F_w}$	Water pumping capacity rate [m^4/h]	$\boldsymbol{v_R}$	Rated wind speed $[m/s]$
$\boldsymbol{v_{mG}}$	Measured wind speed $[m/s]$	$\boldsymbol{v_F}$	Cut-off wind speed $[m/s]$
$\boldsymbol{\sigma_G}$	Standard deviation of the mean measured WS $[m/s]$	$\boldsymbol{P_{eR}}$	Rated electrical power $[kW]$
$\boldsymbol{v_{mS}}$	Satellite-derived wind speed $[m/s]$	$\boldsymbol{P_{e,ave}}$	Average power output $[kW]$
$\boldsymbol{\sigma_S}$	Standard deviation of the mean satellite-derived WS $[m/s]$	$\boldsymbol{Q_w}$	Volumetric flow rate (m^3/day)
$\boldsymbol{f(v)}$	Probability of observing wind speed v	$\boldsymbol{\rho_w}$	Water density [kg/m^3]
$\boldsymbol{g}$	Acceleration due to gravity [m/s^2]	$\boldsymbol{\overline{Sat_i}}$	Mean value of Sat_i

C	Weibull scale parameter [m/s]	$\boldsymbol{H}$	Pump head $[m]$
$\boldsymbol{k}$	Weibull shape parameter $[-]$	$\boldsymbol{\eta}$	System efficiency $[-]$
$\boldsymbol{E_{pf}}$	Energy pattern factor $[-]$	**PVC**	Present value of costs $[XAF]$
$\boldsymbol{MBE}$	Mean Bias Error $[-]$	$\boldsymbol{\eta_{PUMP}}$	Efficiency of the pump $[-]$
$\boldsymbol{RRMSE}$	Relative root mean square error [%]	$\boldsymbol{P_{out}}$	Net hydraulic power output $[kW]$
$\boldsymbol{R^2}$	Coefficient of determination $[-]$	$\boldsymbol{I}$	Investment cost $[XAF]$
$\boldsymbol{Gr_i}$	i^{th} CFD of ground (measured) wind speeds	$\boldsymbol{i_o}$	Nominal interest rate [%]
$\boldsymbol{Sat_i}$	i^{th} CFD of satellite-derived wind speeds	$\boldsymbol{S}$	Scrap value [%]
$\boldsymbol{C_{om}}$	Operation and maintenance costs [%]	$\boldsymbol{I}$	Inflation rate [%]
N	Number of non-zero wind speed data points	$\boldsymbol{r}$	Discount rate [%]
$\boldsymbol{C_{10}}$	Scale parameter at 10 m height agl $[m/s]$	$\boldsymbol{COE}$	Cost of energy $[XAF/kWh]$
$\boldsymbol{C_z}$	Scale parameter at **z** meters height agl $[m/s]$	$\boldsymbol{COW}$	Cost of water $[XAF/m^3]$
$\boldsymbol{E_{WT}}$	Total energy output over the WT lifetime $[kWh]$	$\boldsymbol{IOA}$	Index of Agreement
$\boldsymbol{V_w}$	Annual volume of water [m^3/year]	$\boldsymbol{RMSE}$	Root mean square error $[-]$

ACKNOWLEDGMENTS

The authors gratefully acknowledge the NASA Langley Research Center (LaRC) POWER Project funded through the NASA Earth Science/Applied Science Program for providing wind and temperature data used in this project.

REFERENCES:

1. Mohammed YS, Mustafa MW, Bashir N. Status of renewable energy consumption and developmental challenges in Sub-Sahara Africa. Renew Sustain Energy Rev 2013;27:453–63. https://doi.org/10.1016/j.rser.2013.06.044.
2. IRENA - International Renewable Energy Agency. Global Renewables Outlook: Energy Transformation 2050. Abu Dhabi.: 2020.
3. Fant C, Gunturu B, Schlosser A. Characterizing wind power resource reliability in southern Africa. Appl Energy 2016;161:565–73. https://doi.org/10.1016/j.apenergy.2015.08.069.
4. Hasager CB, Mouche A, Badger M, Bingöl F, Karagali I, Driesenaar T, et al. Remote Sensing of Environment Offshore wind climatology based on synergetic use of Envisat ASAR , ASCAT and QuikSCAT. Remote Sens Environ 2015;156:247–63. https://doi.org/10.1016/j.rse.2014.09.030.
5. Barthelmie RJ and Pryor SC. Can Satellite Sampling of Offshore Wind Speeds Realistically Represent Wind Speed Distributions? J Appl Meteorol 2003;42:83–94.

6. Remmers T, Cawkwell F, Desmond C, Murphy J, Politi E. The Potential of Advanced Scatterometer (ASCAT) 12 . 5 km Coastal Observations for Offshore Wind Farm Site Selection in Irish Waters 2019:1–16. https://doi.org/10.3390/en12020206.
7. Schmidt KM, Swaart S, Reason C, Nicholson S-A. Evaluation of Satellite and Reanalysis Wind Products with In Situ Wave Glider Wind Observations in the Southern Ocean. J Atmos Ocean Technol 2017;34:2551–68. https://doi.org/10.1175/JTECH-D-17-0079.1.
8. NASA. NASA Surface meteorology and Solar Energy: RETScreen Data 2020. https://eosweb.larc.nasa.gov/cgi-bin/sse/sse (accessed September 18, 2020).
9. North Region (Cameroon). From Wikipedia, Free Encycl 2020. https://en.wikipedia.org/wiki/North%7B_%7DRegion%7B_%7D(Cameroon)%7B#%7DClimate (accessed September 18, 2020).
10. Kidmo DK, Danwe R, Doka YS, Djongyang N. Statistical analysis of wind speed distribution based on six Weibull Methods for wind power evaluation in Garoua , Cameroon. Rev Des Energies Renouveables 2015;18:105–25.
11. Mohammadi K, Mostafaeipour A, Alavi O, Goudarzi N, Jalilvand M, Mostafaeipour A, et al. Assessing different parameters estimation methods of Weibull distribution to compute wind power density. Energy Convers Manag 2016;108:322–35. https://doi.org/10.1016/j.enconman.2015.11.015.
12. Mohammadi K, Alavi O, Mostafaeipour A, Goudarzi N, Jalilvand M. Assessing different parameters estimation methods of Weibull distribution to compute wind power density. Energy Convers Manag 2016;108:322–35. https://doi.org/10.1016/j.enconman.2015.11.015.
13. Costa Rocha PA, de Sousa RC, de Andrade CF, da Silva MEV. Comparison of seven numerical methods for determining Weibull parameters for wind energy generation in the northeast region of Brazil. Appl Energy 2012;89:395–400. https://doi.org/10.1016/j.apenergy.2011.08.003.
14. Safari B, Gasore J. A statistical investigation of wind characteristics and wind energy potential based on the Weibull and Rayleigh models in Rwanda. Renew Energy 2010;35:2874–80. https://doi.org/10.1016/j.renene.2010.04.032.
15. Khahro SF, Tabbassum K, Soomro AM, Dong L, Liao X. Evaluation of wind power production prospective and Weibull parameter estimation methods for Babaurband, Sindh Pakistan. Energy Convers Manag 2014;78:956–67. https://doi.org/10.1016/j.enconman.2013.06.062.
16. Azad A, Rasul M, Yusaf T. Statistical Diagnosis of the Best Weibull Methods for Wind Power Assessment for Agricultural Applications. Energies 2014:3056–85. https://doi.org/10.3390/en7053056.
17. Bilir L, İmir M, Devrim Y, Albostan A. Seasonal and yearly wind speed distribution and wind power density analysis based on Weibull distribution function ScienceDirect Seasonal and yearly wind speed distribution and distribution function. Int J Hydrogen Energy 2016;40:15301–10.
18. De Meij A, Vinuesa J-F, Maupas V, Waddle J, Price I, Yaseen B, et al. Wind energy resource mapping of Palestine. Renew Sustain Energy Rev 2016;56:551–62. https://doi.org/10.1016/j.rser.2015.11.090.
19. Stathopoulos C, Kaperoni A, Galanis G, Kallos G. Wind power prediction based on numerical and statistical models. J Wind Eng Ind Aerodyn 2013;112:25–38. https://doi.org/10.1016/j.jweia.2012.09.004.

20. Chang TP. Wind Speed and Power Density Analyses Based on Mixture Weibull and Maximum Entropy Distributions. Int J Appl Sci Eng 2010;8:39–46.
21. Kidmo DK, Danwe R, Djongyang N, Doka SY. Comparison of five numerical methods for estimating Weibull parameters for wind energy applications in the district of Kousseri, Cameroon. Asian J Nat Appl Sci 2014;3:72–87.
22. Neme C. Statistical Analysis of Wind Speed Profile : A Case Study from Iasi Region , Romania 2013;3:261–8.
23. Mohammadi K, Mostafaeipour A, Alavi O, Goudarzi N, Jalilvand M. Assessing different parameters estimation methods of Weibull distribution to compute wind power density 2016. https://doi.org/10.1016/j.enconman.2015.11.015.
24. Ayodele TRR, Jimoh AA a., Munda JLL, Agee JTT. Wind distribution and capacity factor estimation for wind turbines in the coastal region of South Africa. Energy Convers Manag 2012;64:614–25. https://doi.org/10.1016/j.enconman.2012.06.007.
25. Gualtieri G, Secci S. Methods to extrapolate wind resource to the turbine hub height based on power law: A 1-h wind speed vs. Weibull distribution extrapolation comparison. Renew Energy 2012;43:183–200. https://doi.org/10.1016/j.renene.2011.12.022.
26. Mostafaeipour A, Jadidi M, Mohammadi K, Sedaghat A. An analysis of wind energy potential and economic evaluation in Zahedan, Iran. Renew Sustain Energy Rev 2014;30:641–50. https://doi.org/10.1016/j.rser.2013.11.016.
27. Ohunakin OSS, Adaramola MSS, Oyewola OMM. Wind energy evaluation for electricity generation using WECS in seven selected locations in Nigeria. Appl Energy 2011;88:3197–206. https://doi.org/10.1016/j.apenergy.2011.03.022.
28. Adaramola MS, Oyewola OM, Ohunakin OS, Akinnawonu OO. Performance evaluation of wind turbines for energy generation in Niger Delta, Nigeria. Sustain Energy Technol Assessments 2014;6:75–85. https://doi.org/10.1016/j.seta.2014.01.001.
29. Akpinar EK, Akpinar S. An assessment on seasonal analysis of wind energy characteristics and wind turbine characteristics. Energy Convers Manag 2005;46:1848–67. https://doi.org/10.1016/j.enconman.2004.08.012.
30. Paul SS, Oyedepo SO, Adaramola MS. Economic assessment of water pumping systems using wind energy conversions in the southern part of Nigeria. ENERGY Explor Exploit 2012;30:1–18. https://doi.org/10.1260/0144-5987.30.1.1.
31. Rehman S, Halawani T. O, Mohandes M. Wind power cost assessment at twenty locations in the kingdom of Saudi Arabia. Renew Energy 2003;28:573–83. https://doi.org/10.1016/S0960-1481(02)00063-0.
32. Diaf S, Notton G, Diaf D. Technical and Economic Assessment of Wind Farm Power Generation at Adrar in Southern Algeria. Energy Procedia 2013;42:53–62. https://doi.org/10.1016/j.egypro.2013.11.005.
33. Mathew S. Wind energy: Fundamentals, resource analysis and economics. 2007. https://doi.org/10.1007/3-540-30906-3.
34. Ayompe LM, Duffy A. An assessment of the energy generation potential of photovoltaic systems in Cameroon using satellite-derived solar radiation datasets. Sustain Energy Technol Assessments 2013. https://doi.org/10.1016/j.seta.2013.10.002.
35. Ilinca A, McCarthy E, Chaumel J-L, Rétiveau J-L. Wind potential assessment of Quebec Province. Renew Energy 2003;28:1881–97. https://doi.org/10.1016/S0960-1481(03)00072-7.